CHAPTER IV

RESULTS AND DISCUSSIONS

In this chapter, the experimental results of InGaAs QRs grown by droplet epitaxy using MBE are shown. The droplet forming parameters, including the amount of $In_{0.5}Ga_{0.5}$ deposited, the substrate temperature during deposition (T_s), and the Indium-mole-fraction of In_xGa_{1-x} droplets are varied to study their effects on the InGaAs QR properties. By using atomic force microscopy (AFM), the effects of each droplet forming parameters on the size and density of the nanostructures are investigated. Finally, the QRs have been re-fabricated under selected droplet forming conditions with an additional GaAs capping layer for photoluminescence (PL) measurement. The optical properties of the InGaAs QRs have been investigated from PL spectra of the capped InGaAs-QR samples at 20-100 K.

4.1 Evolution of Surface Morphology

The evolution of surface morphology during growth was observed in situ by RHEED and recorded via a commercial CCD camera. Figure 4.1(a) shows the RHEED patterns of a GaAs buffer layer before $In_{0.5}Ga_{0.5}$ deposition. The (2x4) streaky patterns indicate a flat surface of the GaAs buffer layer. During 0-1 minute after $In_{0.5}Ga_{0.5}$ is deposited, the RHEED patterns dim and show no clear streak patterns, as shown in figure 4.1(b). This is attributed to the low density of InGa droplets formed on the surface. During 1-7 minutes after $In_{0.5}Ga_{0.5}$ deposition, the patterns are streaky patterns, as shown in figure 4.1(c). During 7-11 minutes after the deposition, the spotty RHEED patterns in figure 4.1(d) are clearly observed. From the time variation of the RHEED patterns, the mechanism of surface reconstruction can be explained. We can suppose that migration of In and Ga has occurred, causing the merging of neighboring droplets into larger droplets. We also suppose that there is the partial crystallization of droplets. At 11 minutes after the deposition, the crystallization under As_4 flux of 6-7 x 10^{-6} Torr BEP started. The RHEED patterns of QRs which consisted of streaks and spots [57] are shown in figure 4.1(e), indicating the formation of ring-like nanostructures.

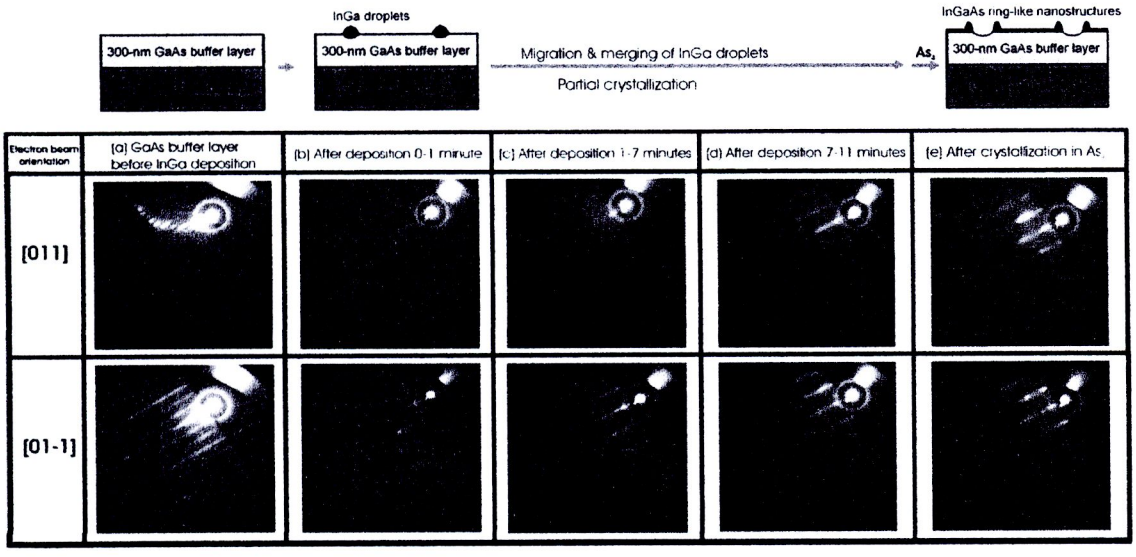

Figure 4.1 The formation process model of InGaAs QRs and RHEED patterns during the growth process. (a) RHEED patterns of 300-nm-thick GaAs buffer layers before $In_{0.5}Ga_{0.5}$ deposition, (b) RHEED patterns of the droplets during 0-1 minute after $In_{0.5}Ga_{0.5}$ deposition, (c) 1-7 minutes, (d) 7-11 minutes after depositing 3 ML $In_{0.5}Ga_{0.5}$, and (e) Streaky and spotty RHEED patterns after supplying As_4 flux of 6-7 x 10^{-6} Torr for 5 minutes, indicating the formation of InGaAs QRs. The incident orientation of electron beam is along the [011] and [01-1] direction.

The final RHEED patterns are different in the case of QD and QR. In the case of QD, the resulted RHEED pattern originates from the product of transmission and chevron pictures, schematically illustrated in Figure 4.2. On the other hand, in the case of QR, the resulted RHEED pattern originates from the transmission/reflection image and the reciprocal picture of the rotational structure, schematically illustrated in Figure 4.3 [57].

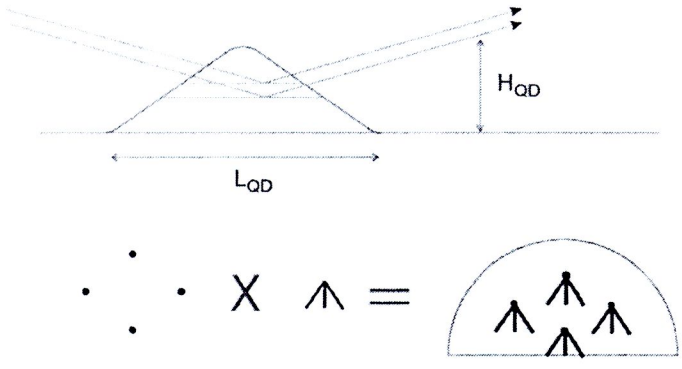

Figure 4.2 Scatterings of grazing electron beam on QD. Upper part: the geometrical arrangement of scattering on several crystal planes in QD. Transmission character dominates here. Lower part: the QD RHEED pattern originated from the product of the diffraction intensity from a crystal cluster and from a pyramid [57].

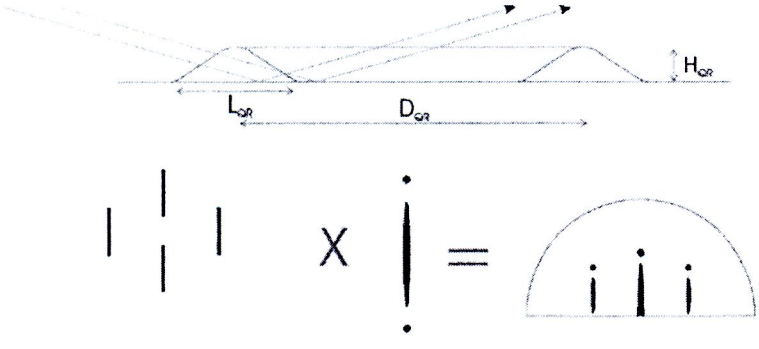

Figure 4.3 Scatterings of grazing electron beam on QR. Upper part: the geometrical arrangement of scattering on several crystal planes in QR or on two-dimensional basis plane. Either transmission or reflection character dominates depending in the finite size. Lower part: the product of transmission or reflection-like intensity and the scattering from rotational-shaped nanostructure resulting in near same RHEED pattern [57].

4.2 Surface morphology

The surface morphology of the crystallized samples was examined by tapping-mode AFM. Low-density InGaAs ring-like nanostructures, so called quantum rings (QRs), are observed. The QRs grown by droplet epitaxy technique have the density in the range of 10^7-10^8 cm^{-2}, which is low-density compared with SK grown QRs (of which density is typically in the range of 10^9-10^{11} cm^{-2}). From reports, the lowest densities of QRs formed by the conversion of SK grown QDs are in the range of ~ $10^9 cm^{-2}$, which is about the lower limit for SK QD formation [1]. Figure 4.4 shows 1000 x 1000 nm^2 2D top-view AFM images of InGaAs QRs grown under different droplet-forming conditions (varying T_s and $In_{0.5}Ga_{0.5}$ amount). The average QR outer diameter (nm), inner height (nm), outer height (nm), and density (× 10^8 QRs per cm^2) for each condition are also included. Note that depth of QRs is equal to different between inner height and outer height. The effects of each parameter are discussed in the next sections.

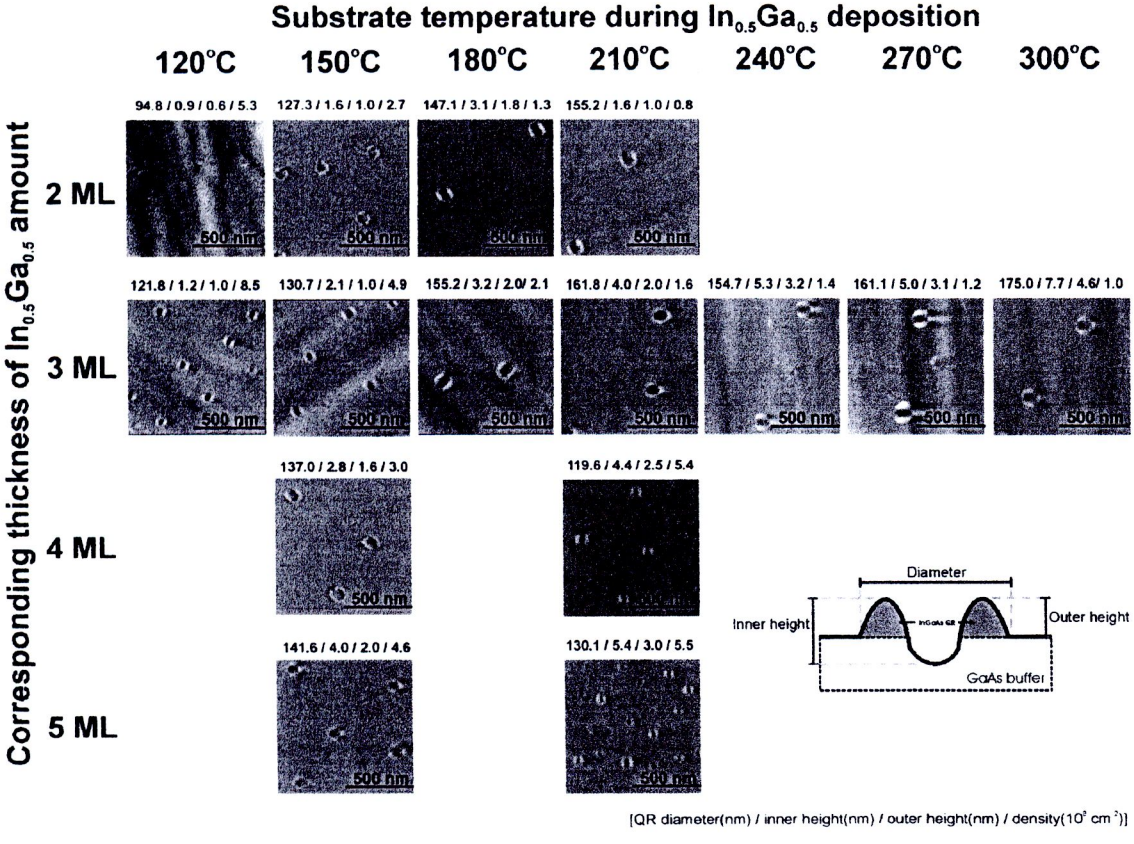

Figure 4.4 1000 x 1000 nm^2 surface morphology of InGaAs ring-like nanostructures grown on GaAs under different growth conditions, including T_s 120-300°C and $In_{0.5}Ga_{0.5}$ amount corresponding to epitaxial layer thickness 2-5 ML.

Figure 4.5 shows an example of 350 x 350 nm^2 surface morphology and the corresponding cross-sectional profiles along the [011] and [01-1] directions of a InGaAs QR grown under the condition of 3ML $In_{0.5}Ga_{0.5}$ deposition and 210°C substrate temperature. The nanostructures are not perfectly circular as seen by the elongation along the [01-1] direction (elongation ratio ~ 1.03-1.28). The elongation is due to anisotropic surface diffusion of group III atoms on GaAs (100) during the crystallization [58,59]. The surface diffusion is much higher along the [01-1] (i.e. surface diffusion coefficient at [01-1] is 4 times larger than that of [011]) due to the atomic corrugation of GaAs (100) induced by the reconstructed dimmer rows. Thus, a valid explanation for the elongation is there seems to be a lot of material *diffused away* along [01-1], also resulting in shallower QRs. Moreover, the center of the QRs is deeper than the substrate surface level due to *drilling effect* of metallic InGa droplets into GaAs matrix after the deposition [5,24]. Note that the QR diameters, the outer heights and the inner heights are obtained from the cross-sectional profiles of the QRs along the [011] direction.

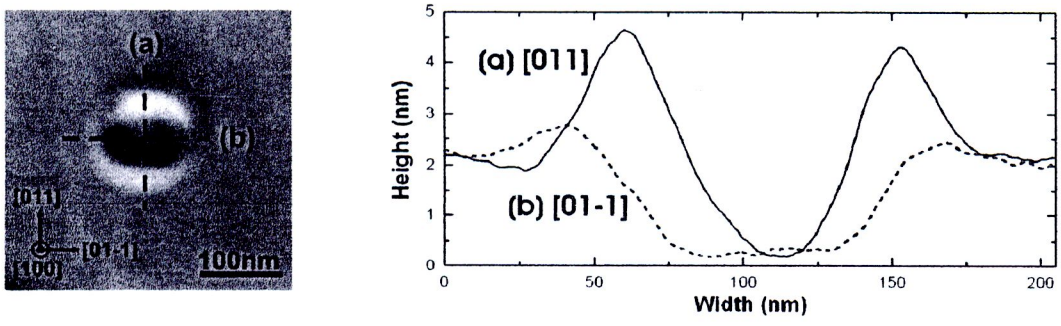

Figure 4.5 350 x 350 nm^2 AFM image and its cross-section along [011] and [01-1] of an InGaAs QR grown at 210°C with 3 ML $In_{0.5}Ga_{0.5}$ deposited.

The appearance of InGaAs ring-structures can be simply described. The formation mechanism of InGaAs ring-shaped nanostructures form metallic InGa droplets are roughly compared to the expansion mechanism of typical liquid droplets. The process is illustrated schematically in Figure 4.6. First, liquid-phase metallic InGa droplets are formed after the deposition of In and Ga atoms on the GaAs substrate (figure 4.6(a)). Like the liquid-phase droplets, the concentration gradient causes the diffusion of In and Ga atoms in the droplets. It results in 2-dimensional expansion of the droplets. At the moment, *drilling effect* of metallic droplets (along with interfacial intermixing process) and partial crystallization occur (figure 4.6(b)). The drilling effect is an etching process at

the interface between group III droplets and underneath III-V surface. At the interface between InGa droplets and the GaAs buffer layer, As atoms (associated with Ga) can be easily soaked into the droplets in order to equilibrate the energy between the GaAs matrix and the droplets. Since As atoms can not exist within the liquid droplets, the As atoms keeps travelling out of the droplets. Then, the As atoms either escape out of the droplets or interact with In and Ga atoms in the droplets, especially at the periphery of the droplets. Hence, InGaAs are formed at this zone, causing partially-crystallized InGa hemispherical-shaped structures [2]. At the same time, InGa droplets keep intermixing with underlying isolated Ga atoms (of which As was sucked out), forming metallic InGa right below the droplets. Second, during the crystallization under As_4 flux, the metallic In and Ga atoms from the droplets diffuse and interact with As atoms supplied on the nearby surface [4] and crystallized into InGaAs (figure 4.6(c)). Again, As atoms can not exist within the liquid droplets, so the efficient crystallization is expected at the bottom edge of the droplets [2,4,24]. As a result, InGaAs ring-shaped structures are formed surrounding the periphery of the droplets [2].

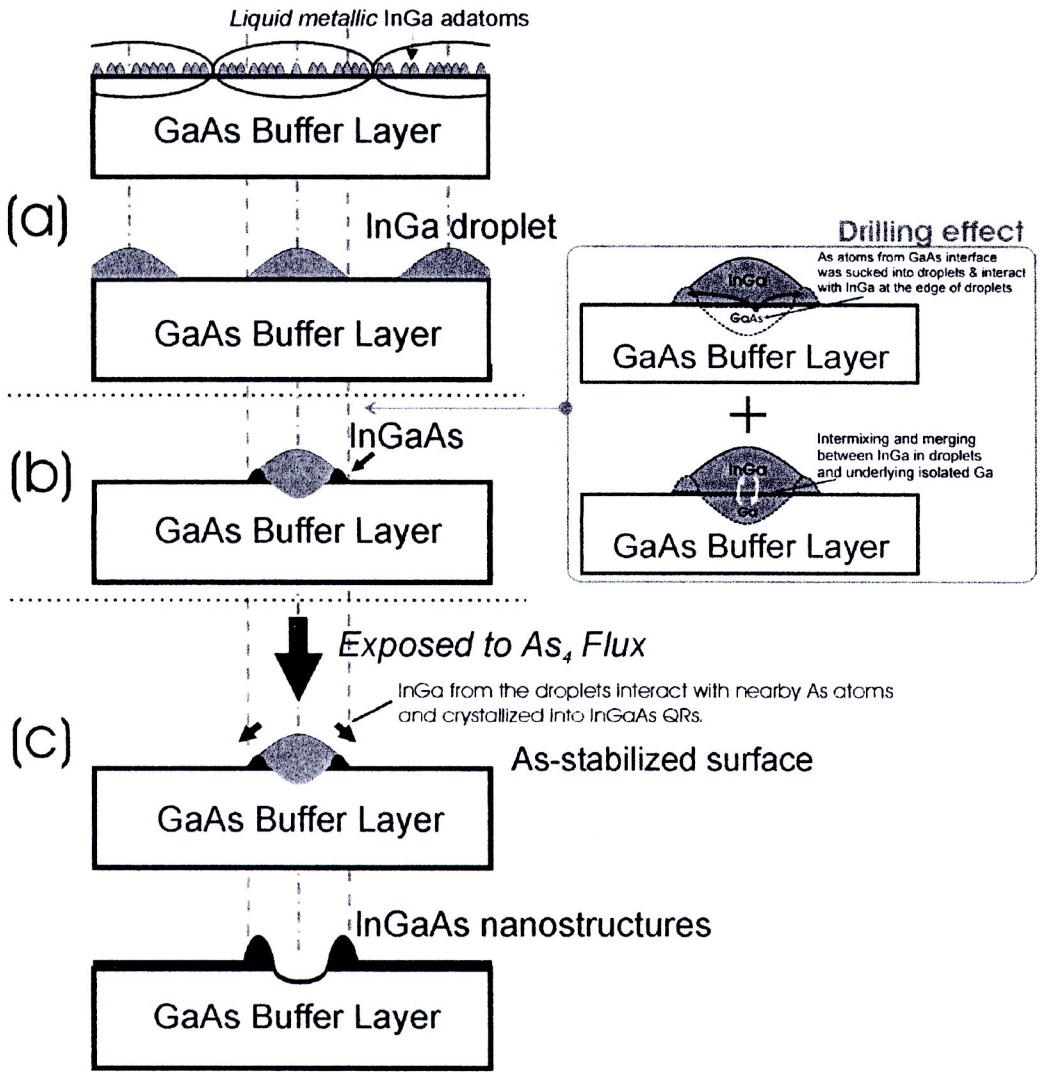

Figure 4.6 The formation mechanism model of InGaAs ring-shaped nanostructures (QRs) from metallic InGa droplets. (a) Formation of liquid-phase metallic InGa droplets from coalescence of deposited In and Ga atoms. (b) Drilling effect of droplets and partial crystallization. (c) The crystallization into InGaAs QRs under As_4 flux (QR diameter ~ droplet diameter).

4.3 Effects of substrate temperature during $In_{0.5}Ga_{0.5}$ deposition: T_s on InGaAs QRs

For the 1st series of samples, the nanostructures were formed under the condition of 2 ML $In_{0.5}Ga_{0.5}$ deposition at T_s = 120, 150, 180, and 210°C and under the condition of 3 ML $In_{0.5}Ga_{0.5}$ deposition on at T_s = 120, 150, 180, 210, 240, 270, and 300°C. Their morphological properties were examined. The dependence of the QR diameter and height on T_s is shown in Figure 4.7.

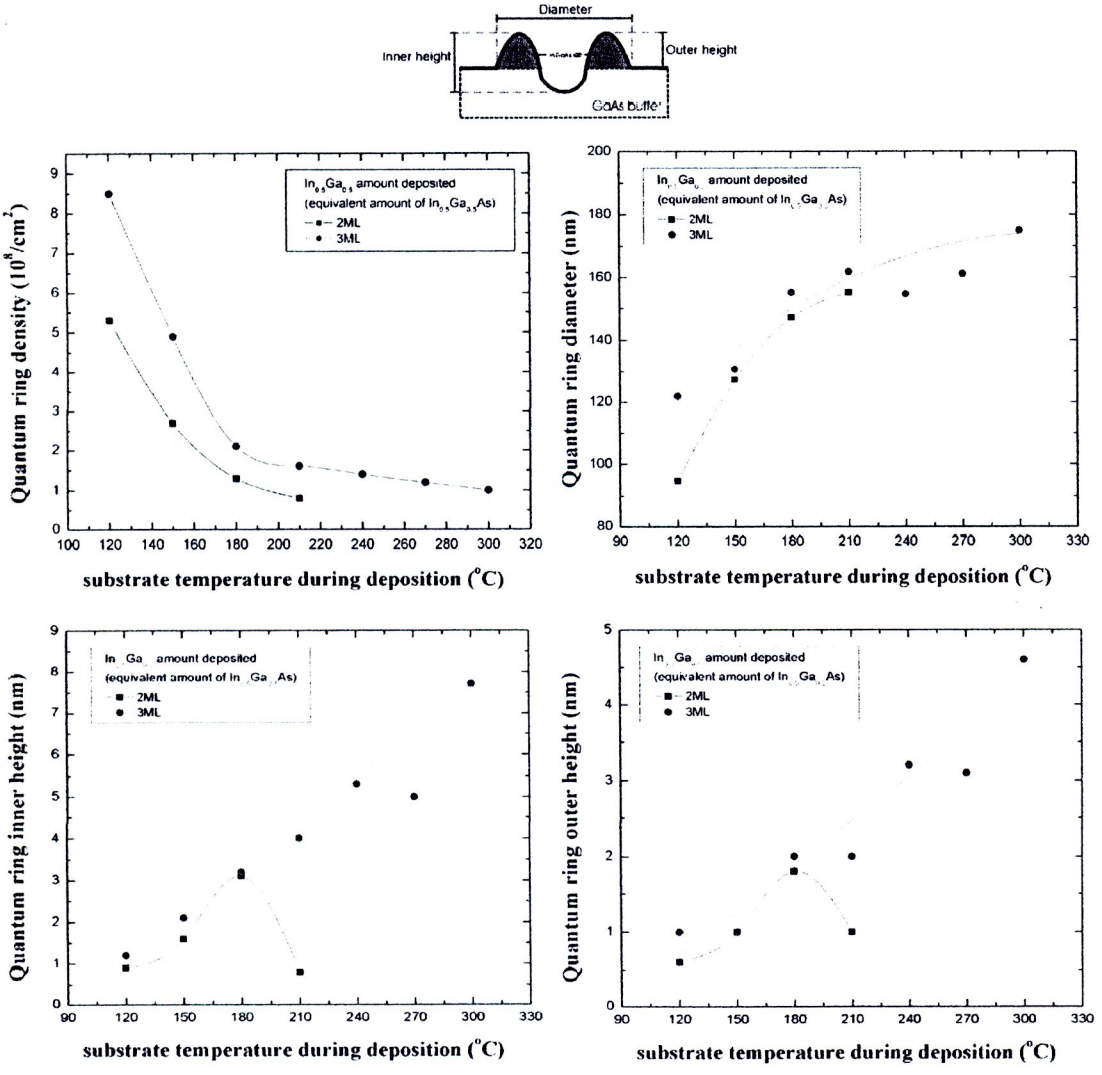

Figure 4.7 The dependence on substrate temperature (T_s) of InGaAs QR average size (diameter, outer height and inner height) and density.

While increasing T_s, the QR average size (typical outer diameter and the height of the QRs along [011]) increases but the density decreases. For example, when T_s = 120°C

under 3 ML $In_{0.5}Ga_{0.5}$ amount condition, the density was 8.5 x 10^8 cm^{-2} with QR diameter ~ 121 nm, the outer height ~ 1.0 nm, and the inner height ~1.2 nm. When T_s = 300°C, the density decreased to 0.9 x 10^8 cm^{-2} with diameter ~ 175 nm, the outer height ~ 4.6 nm, and the inner height ~ 7.8 nm.

The explanation is that the relatively large size of InGaAs QRs is due to the merging of neighbouring metallic InGa adatoms. The surface diffusion ability of metallic In and Ga atoms is proportional to the substrate temperature. Thus, at higher substrate temperature, the merging of InGa adatoms is increased, resulting in greater quantity of InGa in each droplet. After crystallization, fewer but larger InGaAs QRs are formed, as shown in Figure 4.8. Moreover, the increased surface diffusion ability also results in two-dimensional expansion of InGa droplets at high temperature. A schematic drawing of the 150-210°C 2-dimensional expansion is illustrated in Figure 4.9.

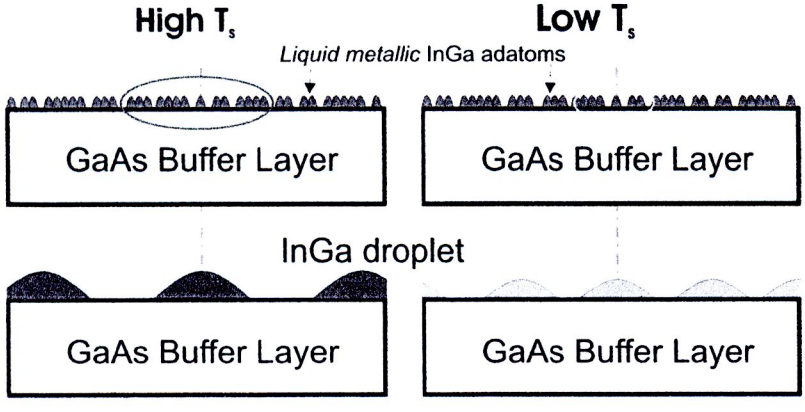

Figure 4.8 An illustration of different merging ranges of neighbouring metallic InGa adatoms at different substrate temperatures, showing larger size but lower density droplets at higher T_s.

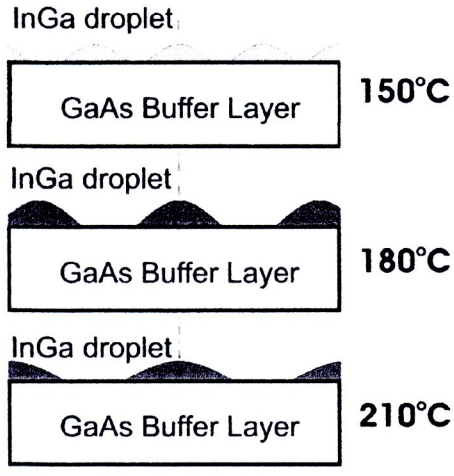

Figure 4.9 A schematic drawing of 2-dimentional expansion of QRs at different substrate temperature 150-210°C, showing wider expansion at higher T_s.

For 2 ML $In_{0.5}Ga_{0.5}$ deposition, we find that the heights of InGaAs QRs decreases at 180°C-210°C. Wider expansion of InGa droplets results in the decreasing of such droplet heights due to the limit of InGa amount deposited.

In addition, the dependence of InGaAs QR structural properties on T_s was investigated using the statistics of QR diameters, the outer heights, and the inner depths as presented in Figure 4.10 [60]. Morphological data of 50 QRs were collected for each T_s. Most InGaAs QRs have larger diameters and higher heights with increasing T_s. The diameter mostly varies between 155~200 nm and the outer height of the rings varies between 1.2~7.5 nm. However, at T_s = 300°C, the diameter distribution spread out more than the distribution at lower T_s. We suppose that *over-migration* of InGa in the droplets may occur at 300°C because of the high surface kinetics. As a result, some In and Ga atoms can migrate easier in-and-out of the droplets and merge with other droplet(s), causing the variation of droplet sizes before crystallization. Indefinitely, the InGa composition of nanostructures may not be entirely uniform due to the different surface kinetics [61]. Most inner depth of InGaAs QRs are virtually the same for various T_s. The inner depths varies between 0~6.5 nm.

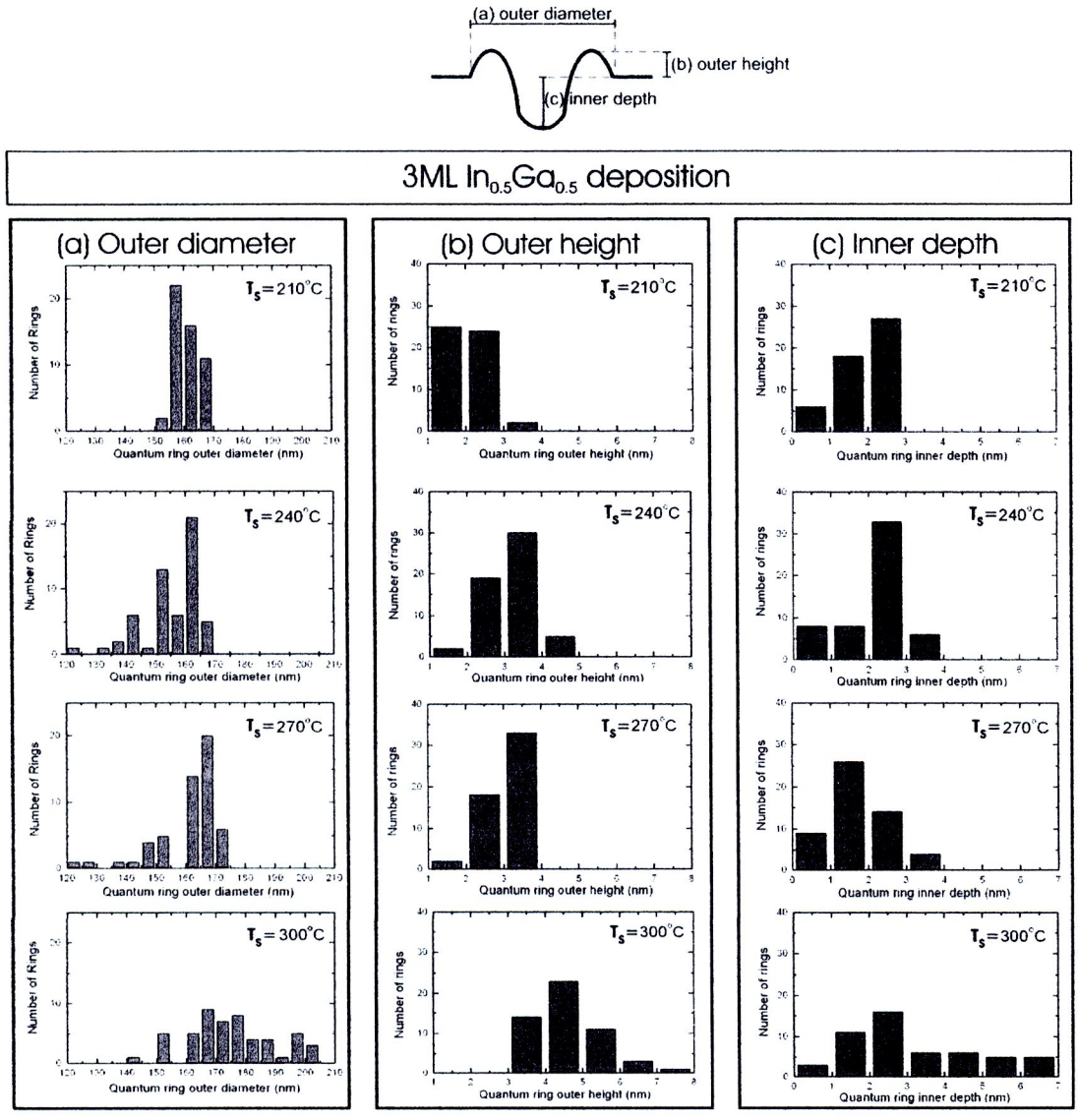

Figure 4.10 Dependence of InGaAs QR diameter, the outer height, and the inner depth on substrate temperature (T_s) during $In_{0.5}Ga_{0.5}$ deposition. The distributions of (a) outer diameter, (b) outer height, and (c) inner depth of InGaAs rings for each T_s: 210°C, 240°C, 270°C, and 300°C (data of 50 rings were collected for each condition) are presented. The $In_{0.5}Ga_{0.5}$ amount is 3 ML with a constant deposition rate of 1 ML/s

4.4 Effects of deposited $In_{0.5}Ga_{0.5}$ amount on InGaAs QRs

For the 2nd series of samples, the QRs were formed under the condition of 2, 3, 4, and 5 ML $In_{0.5}Ga_{0.5}$ deposition at 150°C and 210°C. The morphological properties of each sample were examined for their density and size, as shown in figure 4.11. In the case of 150°C substrate, the QR density oscillates every 2 ML $In_{0.5}Ga_{0.5}$ amount increasing. For 210°C, on the other hand, the ring density tends to saturate after 4 ML $In_{0.5}Ga_{0.5}$ deposition. The QR diameter and the height increase with increasing $In_{0.5}Ga_{0.5}$ deposited amount. However, at 210°C, the diameter decreases after 3-4 ML $In_{0.5}Ga_{0.5}$ deposition.

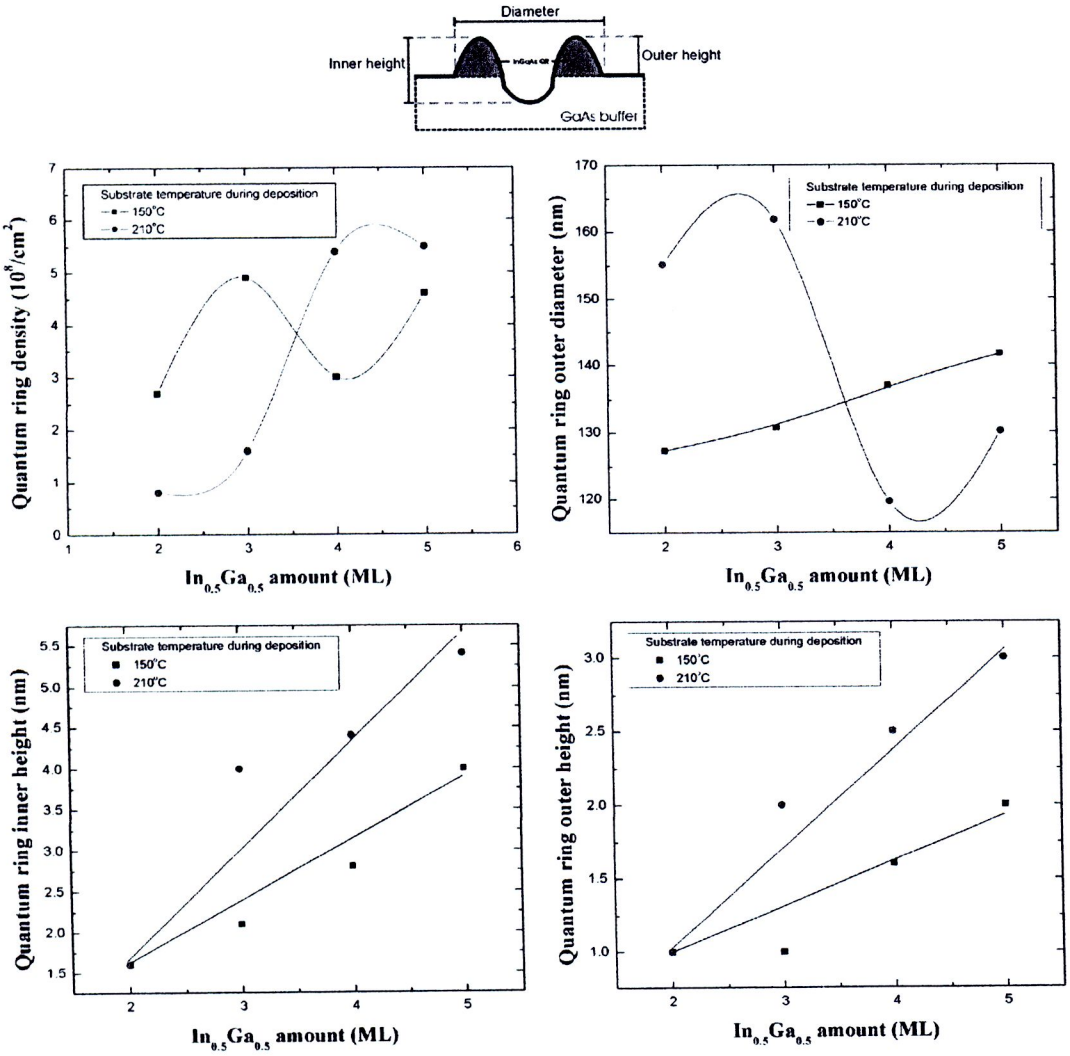

Figure 4.11 The dependence on deposited $In_{0.5}Ga_{0.5}$ amount of InGaAs QR size and density.

Considering the oscillations of QR density at T_s = 150°C, we suppose that there is the merging of metallic droplets into a full-layer. The illustration is shown in Figure 4.12. At the first 2-3 ML $In_{0.5}Ga_{0.5}$ deposited, the density of droplets increasing due to more InGa amount deposited. After the first 3 ML, there are enough small metallic-droplets covering full of the surface. The droplets then coalesce and form an InGa full-layer instead of individual droplets. The newly arrived InGa adatoms would form additional droplets above the layer. Hence, the density of the droplets has been renewed. For T_s = 210°C, on the other hand, the QR density increases during 2-4 ML and tends to saturate after 4-5 ML. Since at the higher T_s (210°C), the droplets are 22% larger but much lower density (70% lower than T_s = 150°C) due to higher surface energy and merging of droplets [see chapter 4.3, effects of T_s]. Therefore, more droplets are required to cover all of the surface. Considering the saturation of QR density, the full-layer takes place after the first 4 ML $In_{0.5}Ga_{0.5}$ deposited. Unlike 150°C, the droplets are so large that the upper part of the droplets still remains above the full-layer when InGa is increased to 5 ML. The newly arrived adatoms would add to the topmost part of the droplets, resulting in a saturation of droplet density. An illustration of each step is shown in Figure 4.13. Also, AFM images and corresponding cross-section of resulted QRs grown at 210°C with 2-5 ML $In_{0.5}Ga_{0.5}$ deposited are shown in Figure 4.14.

In the case of 210°C, the decrease of QR diameter during 3-4 ML is supposed to be caused from accumulated strain. Since the height of the droplets and the outer height of their corresponding InGaAs QRs after crystallization are higher than those of the 150°C case, compressive strain energy is accumulated inside the III-V structures. The relaxation then takes place at the QR-lateral center where the height reaches critical value. Considering hemispherical shape of crystallized QR lateral, when the center of QR lateral relaxes, their surrounding-edges are not relaxed as well (as thickness is not reach critical value as the center). This would limits strain to vertically relax to the top of QR. Thus, the vertical relaxation at center pulls the surrounding edge to the center (of QR lateral) along with increasing height. So, the base-size is forced to decrease with this process.

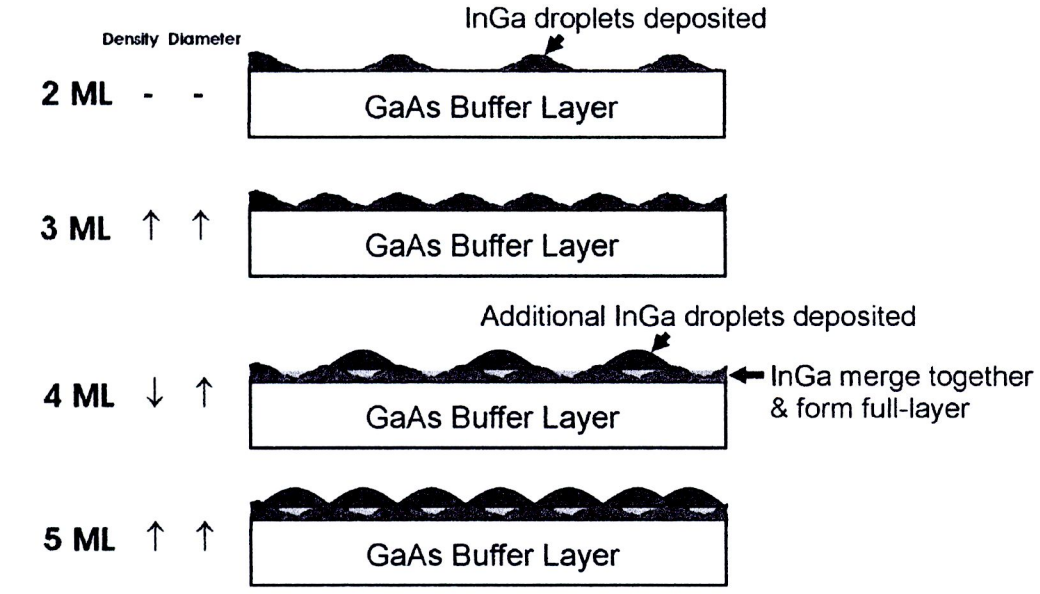

Figure 4.12 A schematic model of the reduction of QR density with increasing InGa amount, for $T_s = 150^{\circ}C$. The details are given in the text.

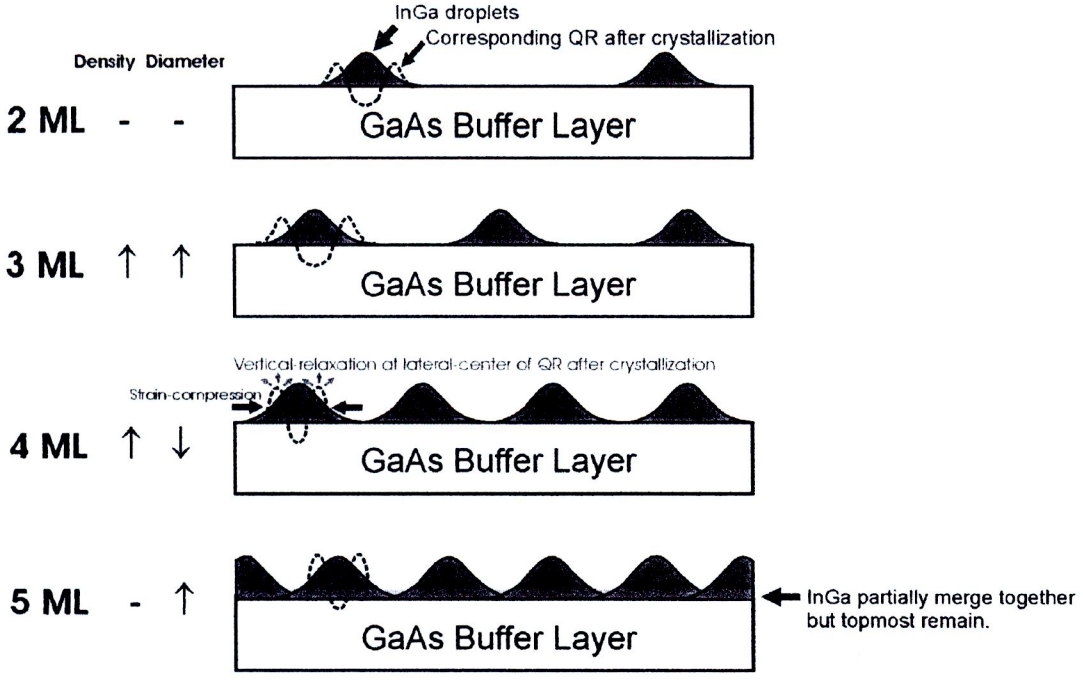

Figure 4.13 A schematic model of the saturation of QR density for $T_s = 210^{\circ}C$, including the drawing of corresponding crystallized QR to briefly describe diameter decreasing from the vertical-relaxation of the accumulating strain. The details of each step are given in the text.

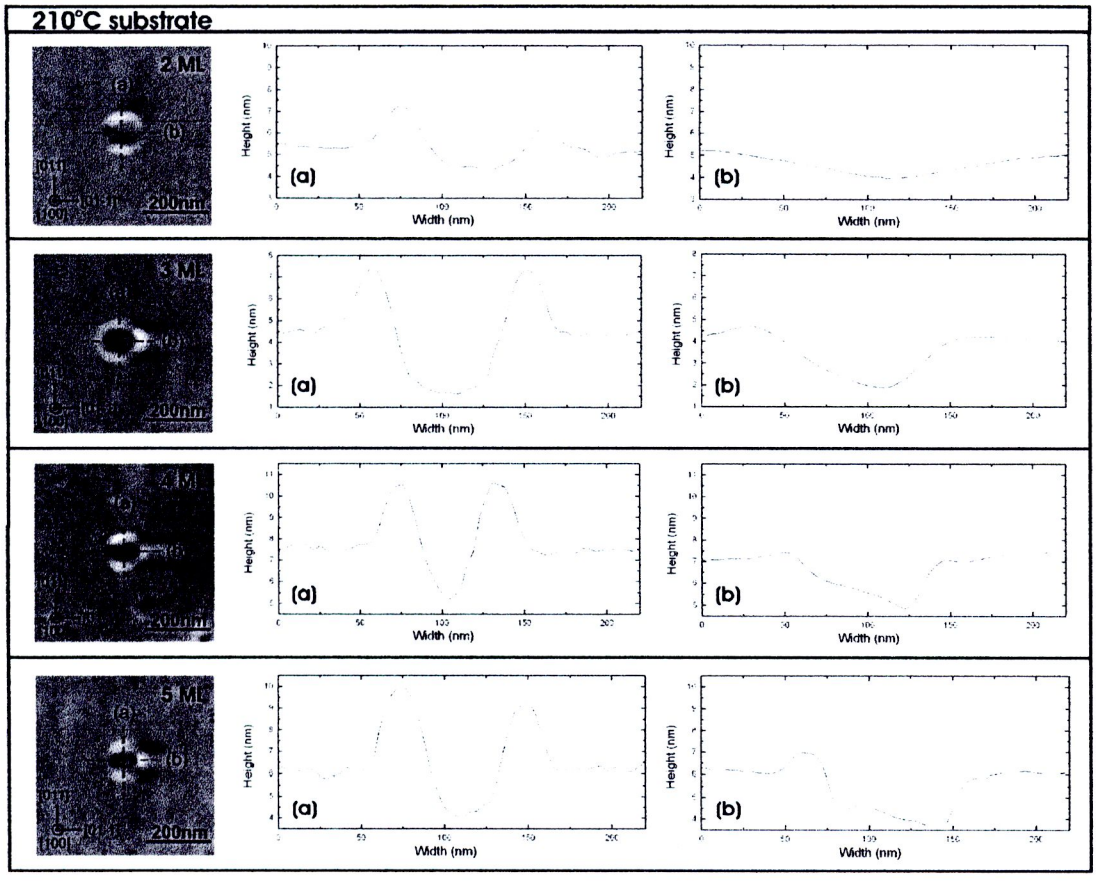

Figure 4.14 500 x 500 nm^2 AFM images and their corresponding cross-section along [011] and [01-1] of InGaAs QRs grown at 210°C with 2-5 ML $In_{0.5}Ga_{0.5}$ deposited.

4.5 Effects of In-mole-fraction of deposited In_xGa_{1-x} on InGaAs QRs

The size and density of the InGaAs QRs are strongly related to the In-mole-fraction (x). Figure 4.15 shows 500 × 500 nm^2 AFM images of the samples grown under the conditions of 3 ML In_xGa_{1-x} amount deposited ($0.3 \leq x \leq 0.7$) at 150°C and the corresponding QR-diameter distributions for each condition. The size of QRs can be clearly classified into 2 groups: subtle tiny-size QRs and obvious large-size QRs. With x = 0.3 and 0.4 (high-Ga-content), most QRs are tiny-size with average diameters of 47 and 58 nm, respectively, while only a few large-QRs exist (average diameter are 72 nm and 78 nm). The density of the tiny-size QRs is much higher than the large-size QR's, as shown in Figure 4.16. However, while increasing x to between 0.5 and 0.7, the density of tiny-size InGaAs QRs rapidly decreases and totally disappears. On the other hand, the

density of normal-size QRs slightly increases. With x = 0.5 - 0.7 (high-In-content), almost only low density large-size QRs are observed. Average QR diameters for x = 0.5, 0.6 and 0.7 are 131, 113 and 114 nm, respectively. The difference between the surface migration lengths of In and Ga atoms [53] is responsible for the difference of QR size and density. With increasing Indium content (x) beyond 0.5, the coalescence of liquid InGa droplets is strongly affected by the surface migration ability of high-In-content droplets. As a result, low density but bigger QRs are formed after crystallization. On the contrast, for x = 0.3 - 0.4, sticky *high-Ga-content* tiny droplets would form high density but tiny QRs after crystallization.

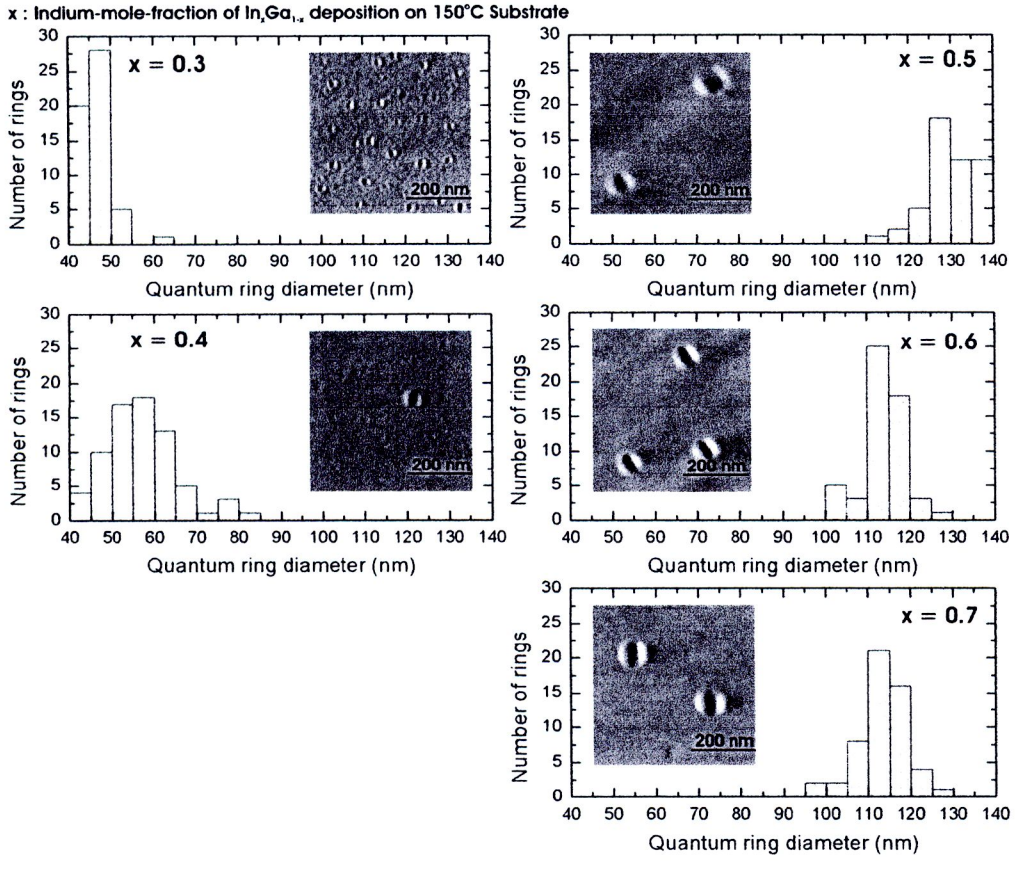

Figure 4.15 500 × 500 nm^2 AFM images of the samples grown under the conditions of 3 ML In_xGa_{1-x} deposited ($0.3 \leq x \leq 0.7$) at T_s = 150°C, including the corresponding QR diameter distributions for each condition.

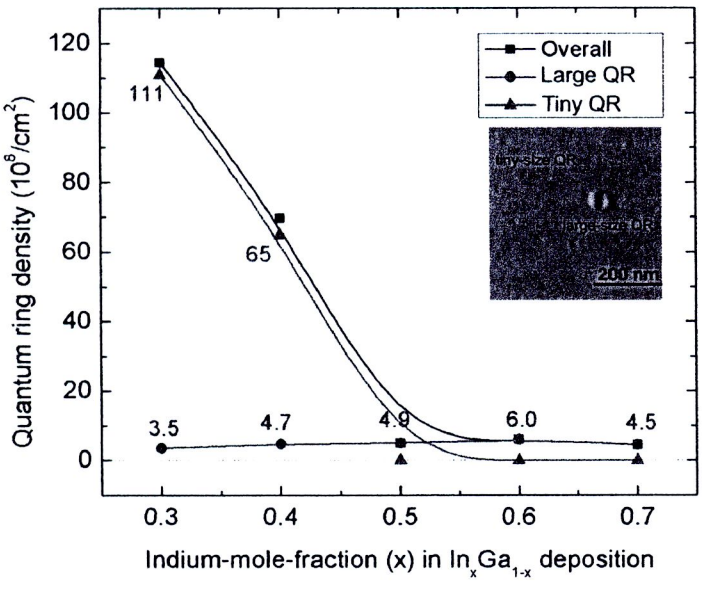

Figure 4.16 The dependence of the density of the tiny-size, large-size InGaAs QRs and overall (including both tiny-size and large-size QRs) on Indium-mole-fraction (x). Deposited In_xGa_{1-x} amount is 3 ML with T_s = 150°C.

4.6 Photoluminescence (PL) measurement of InGaAs QRs

Another set of samples were grown under the droplet forming condition of 2-5 ML $In_{0.5}Ga_{0.5}$ deposition at 210°C with an additional 100-nm GaAs capping layers. The capping layer included 50 ML of GaAs layer grown by migration-enhanced epitaxy (MEE) at 300°C and 310 ML of GaAs layer grown by conventional MBE method at 400°C. The optical properties of the InGaAs QRs were analyzed by PL spectra of the respective samples at 20-100 K.

For PL measurement, a 477 nm Ar^+ laser with power of 20-80 mW is used as the excitation source to characterize the optical properties of the capped InGaAs QRs at 20-100 K. PL emissions for 2 ML and 5 ML conditions are so low that we can not detect any signal from the samples. For 2 ML deposition, the density of QRs (0.8×10^8 cm^{-2}) is very low compared to the other conditions, resulting in very low signal from the sample. For 5 ML deposition, the PL emission efficiency may be degraded due to the accumulation of too much strain. Next, the PL spectra of the capped InGaAs QRs grown under the conditions of 3 ML and 4 ML $In_{0.5}Ga_{0.5}$ droplets deposited on 210°C substrate are examined under a reference measuring condition (exitation power = 40 mW, PL

measuring temperature = 20 K), as shown in Figure 4.17. The PL intensities are relatively low due to low density of the QRs (~ 1.6-5.4 × 10^8 cm^{-2}) and, probably, low-temperature crystallization which results in non-perfectly crystallization of QRs. Under the reference measuring condition, the PL spectra of the sample of 3 ML $In_{0.5}Ga_{0.5}$ droplet centers at 1017 nm (1.22 eV) with respective FWHM of 59 nm (77 meV). For the sample of 4 ML $In_{0.5}Ga_{0.5}$, the PL peak of 1007 nm (1.23 eV) with FWHM of 53 nm (65 meV) is detected. The peak of the 4 ML sample centers at a little shorter wavelength, corresponding with the relatively smaller size of 4 ML-condition QRs. Also, the PL intensity of the sample of 4 ML $In_{0.5}Ga_{0.5}$ is about 3 times higher than that of 3 ML sample, corresponding with the higher QR density (~ 5.4 × 10^8 cm^{-2} for 4 ML condition and 1.6 × 10^8 cm^{-2} for 3 ML condition). The slightly-broadening FWHM is due to 2 reasons; the size distribution of QRs [as shown in section 4.3] and the composition distribution. The composition of In and Ga in InGaAs may not be entirely uniform for all QRs due to randomly intermixing between InGa atoms in droplets and isolated Ga atoms at GaAs buffer interface during the interruption before crystallization [mentioned in section 4.2]. As a result, In and Ga composition are not exactly 0.5.

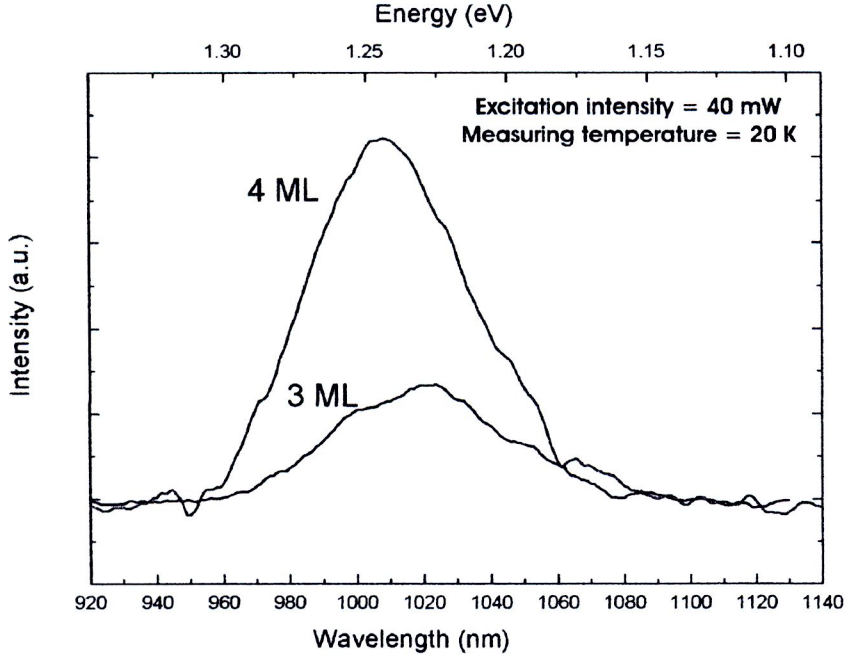

Figure 4.17 The PL spectra of the capped InGaAs QRs grown under the conditions of T_s = 210°C with 3 ML and 4 ML $In_{0.5}Ga_{0.5}$ droplets measured at reference PL measuring condition (laser power = 40 mW, measured at 20 K).

Excitation-power dependence photoluminescence

The PL spectra at 20 K of the samples as a function of excitation power are shown in Figure 4.18. As the excitation intensity increases, the PL intensities increase due to the increase of excess carriers by the excitation power. Also, the PL intensities increase without shifting and broadening while increasing the excitation power. Considering the discrete energy levels of the QR systems, only the ground-state peaks are observed (no state-filling effect). Approximated from the ground-state PL peak position of 1.22-1.23 eV, Indium-content of the QRs can be ~ 0.31-0.50 according to the experimental ground-state energies 1) of InAs/GaAs QDs with a potential well width $\leq$ 4 nm, which is 1.01-1.06 eV [62-65] and 2) of an $In_{0.5}Ga_{0.5}As$/GaAs QDs with well width of $\leq$ 4 nm, which is 1.17-1.23 eV [66,67].

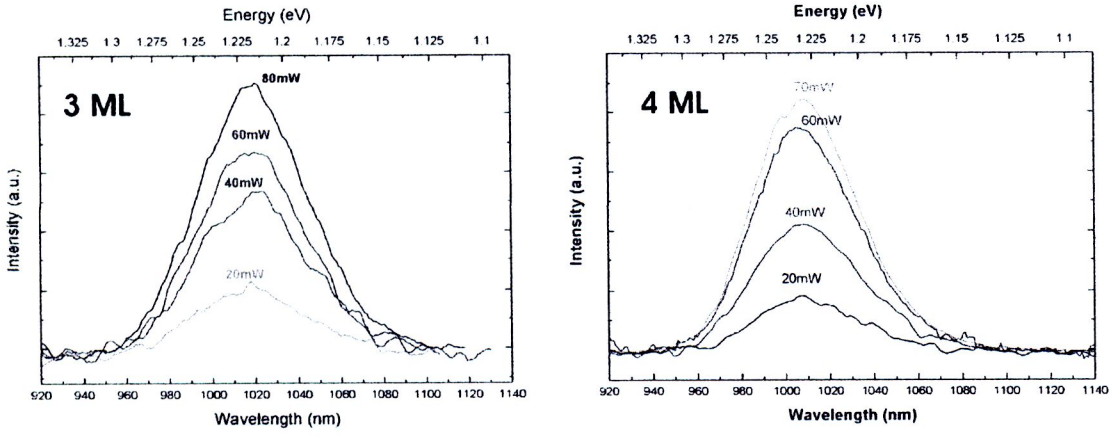

Figure 4.18 The PL spectra at 20 K with 20–80 mW excitation power of the capped InGaAs QRs grown under the conditions of T_s = 210°C with 3 ML and 4 ML $In_{0.5}Ga_{0.5}$ droplets.

Temperature dependence photoluminescence

The PL spectra as a function of measuring temperature are shown in Figure 4.19. The PL intensities decrease while increasing PL measuring temperature. The thermal excitation results in *less stability* of the carriers in QRs [68] and decreases probability of photon emission [69]. The equation used to fit with this result is the simple equation of the activation energy of quantum wells (Farfard et al., 1996)

$$I(T) = \frac{C}{1 + \alpha e^{-\frac{E_A}{kT}}} \tag{4.1}$$

where C is constant, α is a fitting parameter, k is the Boltzmann's constant, and T is the measuring temperature. This equation indicates that PL intensity would decrease with increasing temperature. Even the thermal energy are small compared to the activation energy, there should be a certain part of carrier jump out of the nanostructures due to thermal excitation. By the way, the linewidths are invariant to the temperature change, confirming that thermal broadening is negligible.

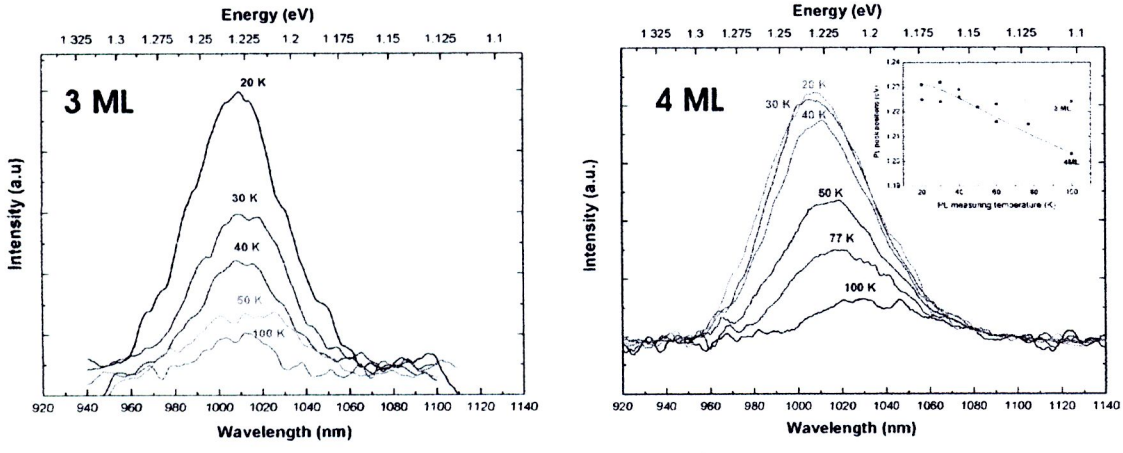

Figure 4.19 The PL spectra at 20-100 K of the capped InGaAs QRs grown under the conditions of T_s = 210°C with 3 ML and 4 ML $In_{0.5}Ga_{0.5}$ droplets (excitation power = 40 mW).

For the sample of 3 ML $In_{0.5}Ga_{0.5}$, the PL peak is *not shifted* while increasing the measured temperature from 20 K to 100 K. It indicates the *strain-free* QRs which create no strain effects on the energy band structures. So, the carriers hardly shift to any energy levels (strain-free may be considered as full relaxation of the thin-lateral 3 ML QRs, while the thicker-lateral QRs of 4 ML can accumulate more strain-field inside). Besides, the coupling properties supposedly support the invariant of the PL spectra to measuring temperature in addition to QR strain-free properties [70]. As shown in Figure 4.20, each of the anisotropic-lateral QRs may act like *coupled-QD*-pair. The QD diameter approximated to the QR-lateral width (~ 30-40 nm) and the distance between the adjacent QDs is ~ 40-50 nm at the center (not coupling) and < 10 nm at the ends (coupling). Overlap of the electronic wave functions in these coupled-like QDs causes a *small splitting* of energy state into two regenerated sub-levels [see section 2.1.2, also, Pauli's exclusion [71]]. Since, the splitting energy (ΔE) depends on inversion of distance between

adjacent QDs ($l_{C\text{-}QD}$), the energy of these two sub-levels is ~ $E_0 \pm \Delta E$, $\Delta E \propto 1/l_{C\text{-}QD}^2$ [39,72-75]. Thus, upon the increasing measuring temperature, the carriers can be thermally-excited to the higher-energy sub-levels, compensating the decreasing bandgap of Varshni's Law [69]. By the way, the small splitting can not be clearly detected in the excitation-power dependence PL due to relatively large FWHM.

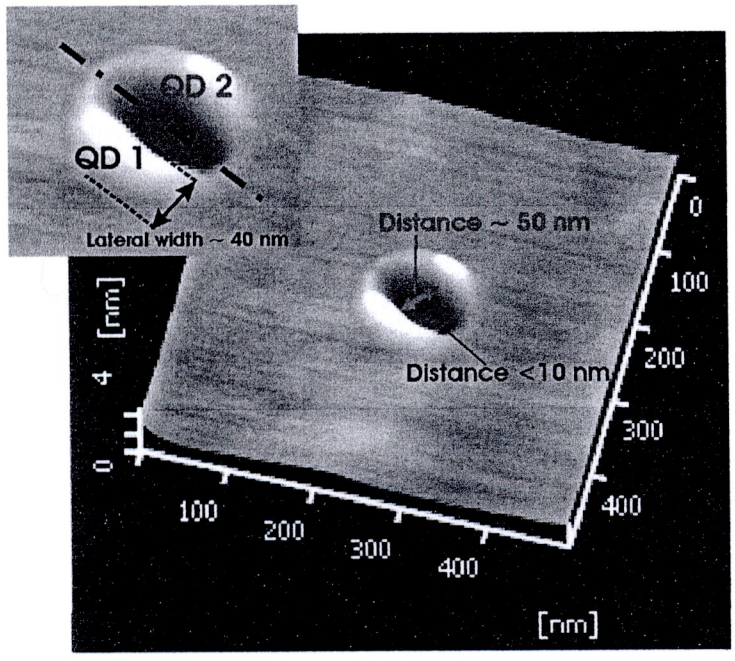

Figure 4.20 3-D AFM image of a QR with the illustration representing coupled-like QD corresponding with the anisotropic-laterals of the QR. The QD diameter is approximate to QR-lateral width (30-40 nm) and the distance between the adjacent QDs is ~ 40-50 nm at the center and < 10 nm at the ends.

However, for the 4 ML sample, the PL peak is 30 meV red-shifted while increasing the measured temperature from 20 K to 100 K. Although the main reason for this shift is the temperature dependence of the bandgap (Varshni's law [69]), the strain field is also supposed to partially accumulate inside the crystallized *thicker-lateral* QRs (higher outer height). The strain can complicate the energy band structures in which excited carriers have less stability [48,76]. This increases the possibility of the carriers to fall to the lower distorted energy levels and emit lower-energy photon with increasing thermal excitation.

Polarized photoluminescence

To characterize PL polarization, a linear polarization analyzer is used to obtain the polarization-resolved spectra. The polarization plane is parallel to (100) plane. The polarized PL spectra are shown in Figure 4.21. The crystal direction of [01-1] with a maximum PL intensity is used as the reference of 0°. On 90° turn of the analyzer from 0°, the intensity deceases to the minimum (called 90°, corresponding to [011] direction). The intensity of the 90°-polarized spectrum (minimum) is 30% less than the 0°-polarized spectrum (maximum). The polarized light is corresponding to the elongation along [01-1] of the QRs, confirming the non-perfect circularity or anisotropy of the QR structures [2,24,60].

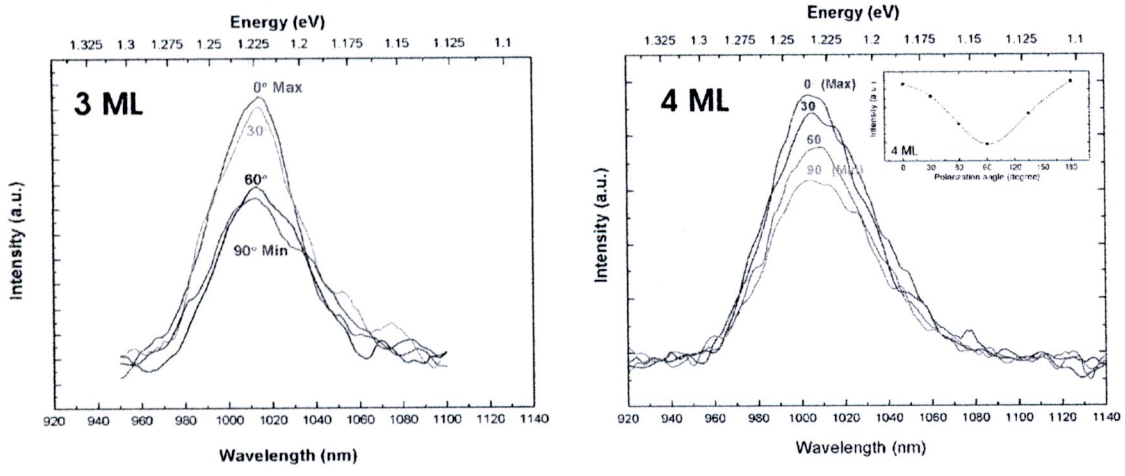

Figure 4.21 The PL spectra at various polarization angles: 0°~[01-1], 90°~[011] of the capped InGaAs QRs grown under the conditions of 210°C substrate with 3 ML and 4 ML $In_{0.5}Ga_{0.5}$ droplets (measuring temperature = 20 K with laser power = 40 mW).